NJC

Accepted Manuscript

This is an *Accepted Manuscript*, which has been through the Royal Society of Chemistry peer review process and has been accepted for publication.

Accepted Manuscripts are published online shortly after acceptance, before technical editing, formatting and proof reading. Using this free service, authors can make their results available to the community, in citable form, before we publish the edited article. We will replace this *Accepted Manuscript* with the edited and formatted *Advance Article* as soon as it is available.

You can find more information about *Accepted Manuscripts* in the Information for Authors.

Please note that technical editing may introduce minor changes to the text and/or graphics, which may alter content. The journal's standard Terms & Conditions and the Ethical guidelines still apply. In no event shall the Royal Society of Chemistry be held responsible for any errors or omissions in this *Accepted Manuscript* or any consequences arising from the use of any information it contains.

ROYAL SOCIETY OF CHEMISTRY

www.rsc.org/njc

Journal Name

RSCPublishing

ARTICLE

Synthesis of CuS flowers exhibiting versatile photo-catalyst response

Cite this: DOI: 10.1039/xoxxoooooox

Muhammad Tanveer[1], Chuanbao Cao[1], Imran Aslam[1], Zulfiqar Ali[1], Faryal Idrees[1], Waheed Samraiz Khan[1], Muhammad Tahir[1], Syed Khalid[1], Ghulam Nabi[2] and Asif Mahmood[3]

Received ooth may 2014,
Accepted ooth may 2014

DOI: 10.1039/xoxxoooooox

www.rsc.org/

Hierarchically structured covellite copper sulfide (CuS) microflowers composed of nanosheets have been successfully fabricated via a one-pot sonochemical process, using copper sulphate and thiourea aqueous solution as precursors in the presence of citric acid, without any prefabricated template. Large-scaled architectures are homogeneous and quite separately displaced and assembled by pure hexagonal single crystalline CuS nanosheets, having thickness within 20nm. The as obtained hierarchical CuS structures possess rather high surface area and the unique double pore size distributions measured from the N_2 adsorption isotherms. Moreover, the possible growth mechanism for CuS hierarchical architectures is proposed on the basis of the temporal evolution controlled experiments. Most importantly, these hierarchically structured CuS catalyst showed highly efficient and versatile photo-catalytic activities as well as excellent recyclability in degrading highly concentrated dyes-aqueous solutions methylene blue (MB), rhodamine B (RhB) and their mixed solution (MB+RhB) with the help of hydrogen peroxide (H_2O_2) under natural light irradiation, suggesting a promising application in wastewater purification.

Introduction

Photocatalysis is a ‘‘green’’ technology for the treatment of organic contaminates and waste water. TiO_2 is undoubtedly the most excellent photocatalyst for the degradation of organic pollutants under UV irradiation. Unfortunately, UV light accounts for less than 5% of the solar energy that reaches the earth surface, which limited the effective use of sunlight for the photocatalytic degradation of organic pollutants. Recently, tremendous efforts have been devoted to develop visible light- driven photocatalysts to maximally utilize the clean, safe and abundant solar energy.[1] However, there are a few successful examples which are visible-light active in the photocatalytic oxidative decomposition of organic contaminants. Among chalcogenide based visible light driven photocatalysts copper sulfide (CuS) is an important transition-metal sulfide, has been the focus of considerable attention not only because of its excellent electrical, optical, physical and chemical properties but also due to its potential applications in many fields, such as superconductor at low temperature, solar energy converter, cathode material, optical filter, gas sensing material and nonlinear optical material.[2-3] It is believed that chemical composition and morphology greatly affects the resulting properties and potential applications of the designed materials. A careful designing approach while controlling size and shape at micro/nano- level gives the opportunity to tailor material properties which are significantly different from bulk materials. In particular, the hierarchical nanostructures have gained increased interest due to several advantages over traditional materials such as low density, high surface area, good permeation and outstanding optical/electrical behaviors,[4-5] which make them promising for their potential applications in drug-delivery systems, lithium-ion batteries, catalysis, gas sensors and absorbents.[6-9] For controlled synthesis of CuS structures, typical methods involved use of several structure directing agents including surfactants and templates (hard (silica, carbon etc) and soft (micelles, emulsions etc) templates).[10-15] However, these methods provide potentially enhanced structures but it is difficult to use such methods at large scale as these include certain complex steps. A potentially more viable method which provides good control over CuS structure has been the use of *in situ* templated “gas bubbles” approach since no template removal step is involved.[16-17] Although, this method provides good control over structure but it lacks wide industrial application due to high cost and time consumption. Despite all these progress, synthesis of well controlled pure phase of CuS with defined shapes and sizes by simple solvothermal method remains a big challenge. Fabrication of CuS hollow structures with hierarchical building units such as nanoplates, nanosheets and nanoplatelets by template free methods is very important but to the better of our knowledge only one report address this synthesis approach for CuS through the ultrasound-assisted aqueous chemical process. However synthesis is achieved by simple method but it is still lacking efficient control due to certain stacking faults in crystal lattice. In this report we address the above mentioned issues in CuS synthesis by using a simple template free sonochemical approach. The hierarchical structures with interior stacked by single-crystal covellite CuS thin nanosheets have been synthesized in the presence of citric acid without use of any templates. In the current report the synthesized nanostructures were examined for their potential applications in industrial wastewater treatment. Water pollution has increased alarmingly in recent years due to presence of certain pollutants

widely used in textile and leather industries. These nanostructures show high activity towards decomposition of pollutants without considerable loss of efficiency (less than 6% after 6 cycles) for highly concentrated dyes (MB, RhB, MB+RhB) aqueous solutions, exhibiting an efficient and versatile heterogeneous catalyst for dyes decolorization. We assume that this work will prove a milestone in optimizing the application oriented synthesis of CuS nanostructures.

Experimental

Sample preparation

The hierarchically structured architectures with well defined and interconnected nanosheets as building blocks were synthesized through a sonochemical pathway without using any surfactant or any prefabricated template. All reagents (analytical-grade purity) used in this work were used without any further purification. In a typical synthesis, 0.25g of citric acid ($C_6H_8O_7$) and 2mmol thiourea (H_2NCSNH_2, TU) were dissolved in 40ml of distilled water then 1mmol of copper sulphate ($CuSO_4.5H_2O$) was dissolved to form a clear solution employing vigorous stirring for 30min. Subsequently, the precursor solution containing autoclave bottle (40mL) was sealed with the attached screw cap to form a closed system, and then transferred into a sonication bath with the temperature of water bath at 80°C without stirring. After the ultrasound radiation was performed for 40min, the reaction mixture solution was cooled naturally for overnight. The resulting precipitate was filtered with a microporous membrane, washed by distilled water, absolute ethanol and acetone several times each and dried in a vacuum at 60°C for 8h for further characterizations. The same typical experiment was repeated several times with different reaction durations to observe a thorough understanding of the architectured synthesis of CuS.

Characterization

The phase purity and crystal structure of the products were examined using X-ray diffraction (XRD, PhilipsX'pert Pro X-ray diffractometer) equipped with 1.5406Å Cu Kα radiations, whereas, the surface morphologies and compositional characterizations were ascertained by scanning electron microscopy (SEM, Hitachi TM-1000), energy dispersive x-ray spectroscopy (EDS) and a high-resolution transmission electron microscope (TEM, JEOL JEM-2010). The X-ray photoelectron spectroscopy (XPS) spectra were recorded on a Rigaku XPS 7000 spectrometer using non monochromatic Mg K (alpha) (1253.6eV) at a source of 200W, chamber pressures during the measurement was about 10^{-7}Pa. The binding energies were referred to the adventitious C 1s peak at 284.6eV. Optical properties of the sample were studied at room temperature using ultraviolet– visible–near infrared (UV–vis–NIR) transmittance spectrophotometer (U-4100) and photoluminescence properties were visualized by F-4500 fluorescence spectrophotometer. The Brunauer–Emmett–Teller (BET) specific surface areas of the powders were analyzed by nitrogen adsorption in a Micromeritics ASAP 2020 nitrogen adsorption apparatus (USA). All the samples were degassed at 150°C before nitrogen adsorption measurements in the relative pressure (p/p_0) range of 0.05–0.3. The Brunauer–Emmett–Teller (BET) method was utilized to calculate the specific surface area; pore volume and pore diameter distribution was derived from the adsorption isotherms.

Photo-catalytic activity evaluation

MB and RhB are considered to be the popular probe molecules in heterogeneous catalytic reactions. For the evaluation of catalytic activity at ambient temperature, a series of comparative experiments were carried out under natural light for de-coloration with the assistance of hydrogen peroxide (H_2O_2). The original solutions of MB or RhB were separately prepared by adding 1.5mL H_2O_2 (30%, w/w) and 3mL MB or RhB solution (400mgL^{-1}) in 100mL of de-ionized water, then 20mg of the as-prepared CuS hierarchical microflowers were added and the solution was magnetically stirred in the dark for 30min to ensure the establishment of an adsorption–desorption equilibrium before illumination. Afterwards, the dispersion was irradiated by natural light during continuous magnetic stirring and during given time intervals, about 3mL of the suspension was taken from the reactor and centrifuged to separate the catalyst. The UV–vis absorption spectra were recorded at different intervals and the characteristic absorption peaks at 604nm for MB and 553nm for RhB were monitored to follow the catalytic degradation process. As a comparison, the photo-catalytic activity of the dense commercial CuS powder (Degussa Co.) was tested in the same experimental conditions. Moreover, for the stability measurement the same materials were centrifuged from the solution and above mentioned steps were repeated. The catalytic decolorization of the dye solution is a pseudo-first-order reaction and the degradation rate of is calculated by the following formula.[18]

Degradation (%) = $(1 - C_t/C_o) \times 100\%$ (1)

Here, C_o and C_t indicate the initial concentration of the dye and the concentration at time t. Furthermore, to demonstrate the variety of degradation by the CuS microflowers, in a similar way the mixed solution of (MB+RhB) was prepared and above mentioned steps was repeated for degradation and stability measurements.

Photoelectrochemical measurements

Indium-tin oxide (ITO) glass was selected as the working electrode, cleaned by sonication in cleanout fluid, acetone and ethanol for 10 min each. A thin film was fabricated on the ITO substrate having area 1 cm^2 with the help of PVDF in NMP solution. After pasting the product on ITO coated glass substrate it was annealed at 120 °C for 8 h under vacuum. Subsequently, the uncoated part of the ITO glass was isolated with epoxy resin. The photocurrent was measured by a conventional three electrode electrochemical cell with a working electrode, a platinum foil counter electrode and Ag/AgCl (3MKCl) as a reference electrode. The working electrode was immersed in a sodium sulfate electrolyte solution (0.2 M) and irradiated by a 500 W xenon lamp from the back side in order to minimize the influence of the thickness of the semiconductor layer. The light/dark short circuit photocurrent response was recorded with a BAS Epsilon workstation. Electrochemical Impedance Spectroscopy (EIS) experiments were carried out on a ZENNIUM electrochemical workstation (Zahner, Germany). EIS was used to evaluate the properties of photocatalysts under AC polarization, and was conducted in a frequency range of 100 mHz to 100 KHz with an amplitude of 5 mV in the DC Open Circuit Potential (OCP) after a 10 min delay.

Results and Discussion

Structural and morphological characterizations

The X-ray diffraction test was employed to understand the identity and phase purity of as-resulting products. As depicted in Figure 1, the strong and sharp diffraction peaks suggest that the as obtained product is well crystalline. The entire diffraction peaks match well with the standard data of covellite-type CuS with hexagonal lattice parameters of a= 3.7920Å, b= 3.7920Å and c= 16.3440Å (covellite, syn, JCPDS No: 00-006-0464).

The XRD pattern shows that the product is devoid of any detectable impurities or any other copper sulfide phases. The energy-dispersive spectra (EDS) analysis of the as prepared product shown in the inset of Figure 1 demonstrates that the chemical components only consist of Cu and S elements with an atomic ratio (Cu: S= 1:1), in agreement with the above XRD result.

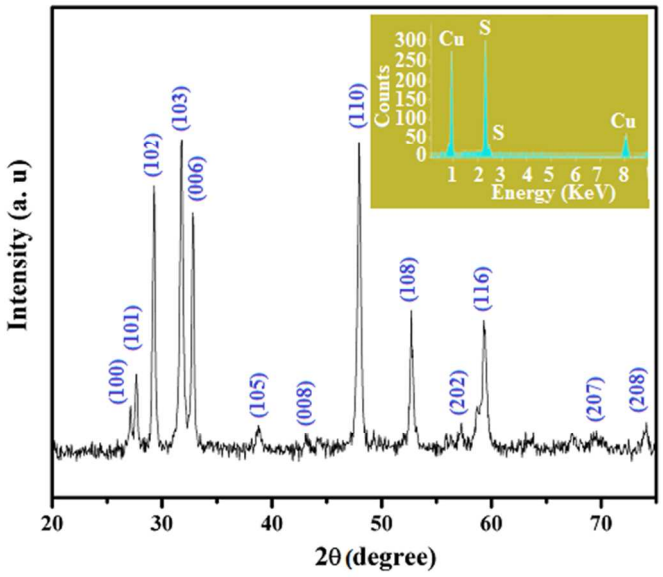

Figure 1. XRD spectrum and EDS spectrum (inset) of CuS microflowers.

X-ray photoelectron spectroscopy (XPS) analysis of the as synthesized CuS hierarchical microflowers was carried to analyze the chemical composition, purity of the prepared sample and to identify the chemical status of Cu element in the sample.

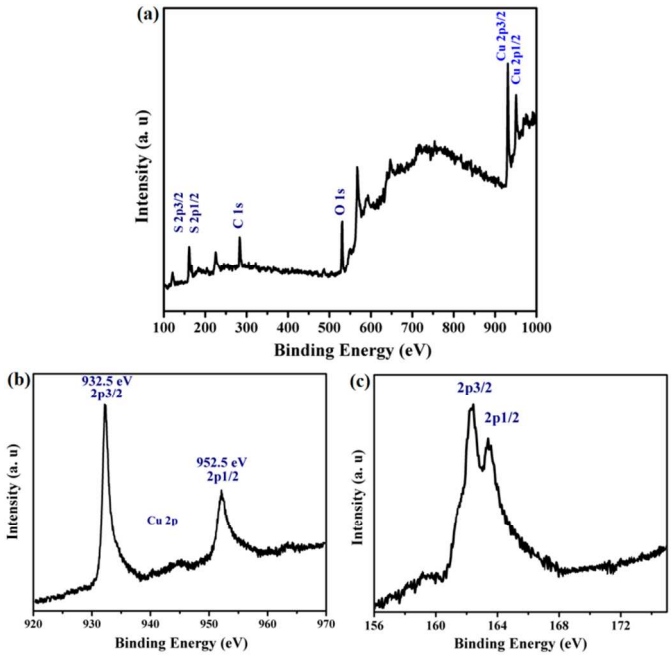

Figure 2. XPS spectrum of the as-synthesized CuS microflowers (a) XPS spectra of survey of the as-synthesized CuS microflowers, (b) XPS spectra of close-up survey in the Cu 2p region, (c) XPS spectra of close-up survey in the S 2p region.

Figure 2a exhibits the XPS full survey spectrum, the presence of Cu peaks of Cu 2p, S 2p, O 1s, and C 1s can be clearly observed. The weak peaks of O and C come from H_2O, O_2, and CO_2 adsorbed on the surface of the sample and adventitious hydrocarbon from XPS instrument itself, respectively.[19] Figure 2b is representing high resolution spectrum of Cu 2p, the high-resolution spectra in the Cu 2p region revealed the presence of two strong peaks. It is obvious that the presence of two strong peaks separated by 20.0eV at 932.5eV and 952.5eV for Cu 2p3/2 and Cu 2p1/2, respectively, are essentially identical binding energies for the Cu 2p orbital in accord with Cu(II).[19] In addition, a small chemical shift about (0.3eV) has occurred compared to the elemental copper. Meanwhile, two shakeup satellite lines at 943.1 and 963.4eV are observed, which are the characteristic of materials having d(9) configuration in the ground state, that is, Cu(II),[20] indicating the paramagnetic chemical state of Cu^{2+} Furthermore, symmetrical shapes of the two Cu 2p XPS peaks also imply the presence of pure CuS. In Figure 2c, the high resolution survey at the S 2p region shows the presence of two peaks at 162.3eV and 163.2eV, all these peak positions are well matched with literature.[21] The Cu/S ratio was calculated from the peak areas of Cu and S-cores, the value was found to be 1.02 that is closely matched with the Cu/S value estimated from EDS analysis.

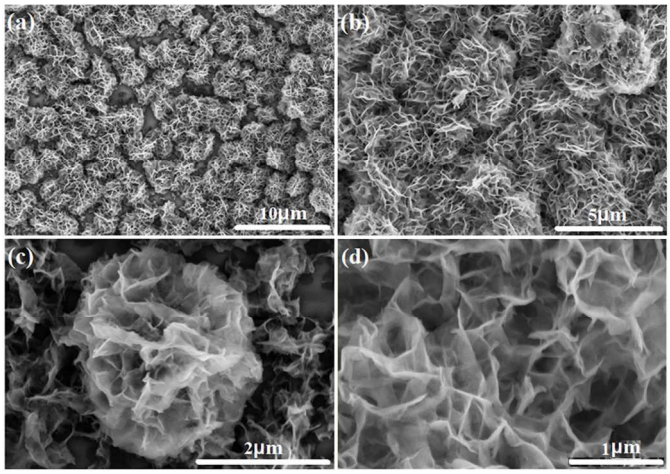

Figure 3. (a, b, c, d) SEM images of CuS hierarchical microflowers.

Figure 3 displays the typical SEM images of the as prepared hierarchical microflowers of CuS with nanosheets building blocks at different magnifications. From the low-magnification SEM result (Figure 3a), it is obvious that CuS Microflowers have high yield, the excellent hierarchical architectures with amazingly well defined and interconnected unique nanosheets as building blocks at large scale. The images in Figure 3a, b clearly indicate shape and size consistency and high yield of the product, all of the microflowers are well defined, quite consistent and separately displaced. In the corresponding magnified image in Figure 3c, d it can also be ascertained the microflowers are architectured identically with extremely thin nanosheets, much complex, hollow in nature and nanosheets are well interconnected. Moreover, there are a lot of cavities among the individually and hierarchically connected nanosheets within each entirely isolated microstructure. The hierarchically connected nanosheets are few nanometers in thickness and interconnected identically to create deep and capacious pores within the entire complex architecture of CuS Microflower. Further detailed investigations of crystallographic features of as prepared CuS microflowers were performed by TEM and HRTEM. Figure 4a displays the TEM image of the as prepared microflowers, the strong

contrast between the dark edge and pale portions is the obvious evidence of cavities within the entire architectures.

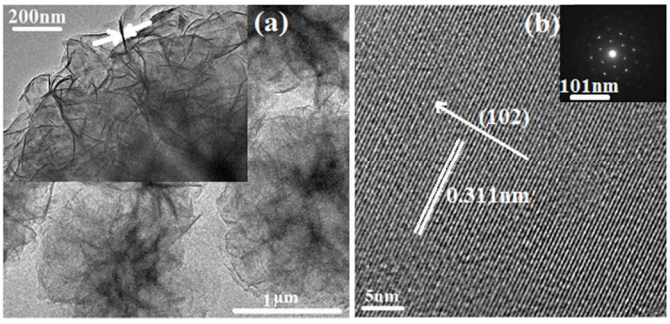

Figure 4. (a) TEM image of as synthesized CuS Microflowers, (inset is the high magnification TEM image of CuS Microflowers) (b) HRTEM image of CuS Microflowers, (inset is the SAED pattern of CuS microflowers).

From the high magnification TEM image of microflower (inset of Figure 4a), it is obvious, that each hierarchical structure is entirely composed of nanosheets having thickness 18nm approximately and joined in a well defined manners within each micro architecture of as synthesized CuS microflower, being in agreement with SEM results. The HRTEM image conducted on the scattered nanosheets is displayed in Figure 4b. From the top view of HRTEM image, the regular spacing of the clear lattice planes is calculated to be 0.311 nm, which is in good agreement with the interlayer spacing's of (102) crystallographic plane of hexagonal CuS.[22] The formation of microflowers started from a nucleus, as soon as the reaction parameters reached the optimized condition. These nuclei started growth in specific directions to form nanosheets which then join together to form highly connected structures by self assembly involving bending and aggregation.[23] Furthermore the well-defined spots in the SAED spectra (Figure 4b, inset) illustrate the perfect growth of single crystals of CuS. Thus, these observations confirmed that CuS microflowers have same crystallographic orientation along the nanosheets axis as a perfect single crystal.

Plausible formation of hierarchical microflowers of CuS

The complex of Cu^{2+} with thiourea is readily formed owing to availabitliy of lone pair of electrons on ligand and free states of metallic ions. Upon heating, these complexes decompose to give carbon dioxide (CO_2), free Cu^{2+} ions and active S^{2-} ions into the aqueous solution. This provides the basis for reaction between Cu^{2+} and S^{2-} to form CuS. The chemical reactions can be expressed as:[24-26]

$$Cu^{2+} + xTU \rightarrow Cu(TU)_x^{2+} \quad (2)$$

$$TU + H_2O \rightarrow CO_2 + 2NH_4^+ + S^{2-} \quad (3)$$

$$Cu^{2+} + S^{2-} \rightarrow CuS \quad (4)$$

Use of sonochemistry to achieve short lived conditions such as high temperature (>5000 K), high pressure (>20 MPa) and very fast cooling rates (10^{10} Ks^{-1}) provide with the opportunity to develop well defined products which are not possible by other methods. The formation of bubbles in the reaction chamber for short interval of times acts as a trap for the Cu complex. During collapsing of bubbles, entrapped water is changed into ionic states which boost the decomposition of entrapped Cu complex resulting in formation of CO_2 and S^{2-} anions. The Cu^{2+} and S^{2-} now react to give the product. This method has been used widely to obtain covellite phase of CuS in the open system.[27-28] Using similar synthesis conditions provided aggregated nanoparticles when reaction was carried out in the open system for different reaction durations (Figure S1a, b, c, d) employing sonochemical synthesis. The growth was also studied under hydrothermal conditions where spherical particles of CuS were observed upon prolonged reaction times. At short reaction times, a disordered structure was obtained with increasing order upon increase in reaction duration. An ordering of the structure with increase in reaction duration suggests the need of more time for the directional growth (Figure S2a, b, c, d). It is demonstrated clearly that the hierarchical structure of CuS with well defined cavities cannot be fabricated under the ambient air by sonolysis and through the hydrothermal process. The growth of CuS was then studied in a pre-designed closed sytem. This closed system gave better control over the synthesized structure due to inherent retention of CO_2 in the reaction chamber. Sonolysis led to the formation of bubbles which act as nucleation centers where CuS crystals started to grow. As shown in Figure S3a, when the reaction was carried out for shorter duration of time (~10min), the product lack any clear morphology which demonstrates that reaction is still in "initiation stage". However, upon increase in reaction duration, CuS nanograins join together to form hollow hierarchical and randomly aggregated structures (Figure S3c, d). Further increase in reaction time to 30min led to symmetrical hierarchical architectures with well defined cavities. When the reaction time was increased to 40min, the CuS structures gradually dissolved giving rise to integrated porous submicrospheres. It can be assumed that CuS crystals grow in the nucleation sites inherently produced by sonolysis. Inhibition of CO_2 escape from reaction chamber provides additional structure directing species which then helps in aligining the growing CuS crystals in specified directions as demonstrated by HRTEM analysis and XRD diffraction patterns. The XRD analysis of all synthesized products at different reaction stages provide further evidence that all the products consist of pure covellite phase of CuS whose intensity increase with increasing reaction time (Figure S4). This depicts the improving crystallinity of products with increasing reaction times. The walls of hollow and hierarchically architectured microflowers are composed of intersecting nanosheets along with well defined cavities, which are determined by the intrinsic crystal characteristics of the hexagonal CuS.[29-31] the nanosheets building blocks are attributed to the presence of citric acid ($C_6H_8O_7$) in the reaction system. Since citric acid is not only a strong chelating agent with metallic cations, it acts as an anionic surfactant in the reaction system as well.

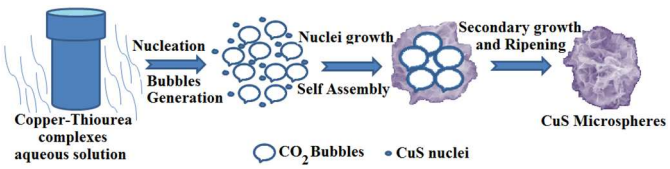

Figure 5. Growth mechanism for the formation of CuS microflowers.

Recently it has been excellently ascertained in the literature that for the growth of hydroxyapatite, citric acid can bound powerfully with metallic cations through its carboxylate groups[32-34]. In presence of citric acid a large quantity of $[Cu(C_6H_5O_7)_4]^{-10}$ is produced within the reaction system, which have a high negative charge. So, the two-dimensional growth of CuS with the building blocks of the microflowers is promoted quite obviously due to preferential absorption of this negatively charged moiety along some positive polar plane[35]. This might be an authentic reason for the generation of planner nanosheet building units of microflowers in the presence of citric acid. Based on the above analysis and results, the schematic diagram and plausible formation mechanism for hierarchical CuS

hollow structures is illustrated in Figure 5. Considering as, a sonohydrolysis, oriented aggregation, secondary growth, ripening process, primary particles followed by a slow aggregation and crystallization of primary particles.

Optical properties and BET surface area

UV–Vis absorption measurement is one of the most important methods to reveal the optical properties of semiconductor nanocrystals. The UV–vis absorption spectrum of unusual and complex architectures of CuS hierarchical microflowers is shown in Figure 6a. The absorption spectrum exhibited a characteristic covellite CuS like absorption band in the near-IR region,[36-38] due to inter band transitions (absorptions) from valence states to the unoccupied states.[37]

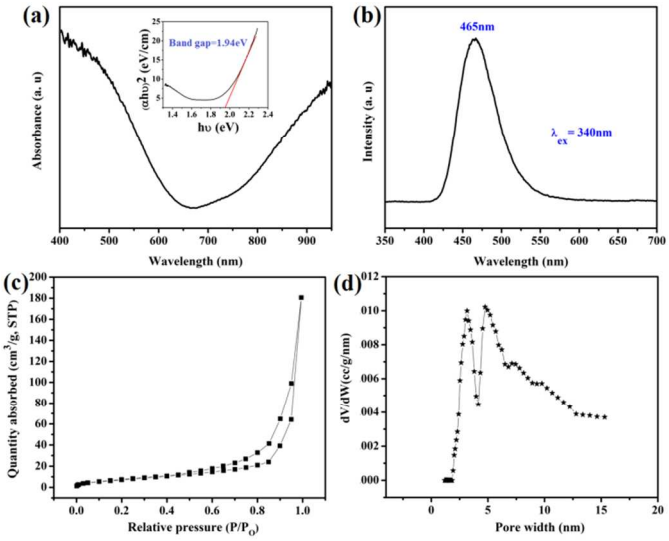

Figure 6. (a) UV-visible absorption spectrum, Band gap energy (inset) of as prepared CuS complex architectures, (b) PL spectrum of as-prepared as prepared CuS hierarchical architectures, (c) Nitrogen adsorption-desorption isotherm of the as-synthesized CuS microflowers, (d) pore size distribution curve of as prepared CuS microflowers.

Compared with bulk covellite CuS[38], the as prepared nanosheet based hierarchical microflowers exhibits a large and distinct blue-shift, which is possibly attributed to the quantum confinement effect of the thinnest CuS nanosheets comprising the entire microstructure. Moreover, according to the equation $\alpha E_p = K(E_p - E_g)^{1/2}$, a plot of $(\alpha E_p)^2$ Vs E_p based on the direct transition of as prepared product is shown in the inset of Figure 6a, the extrapolated value of E_p at R= 0 gives absorption edge energies correspondence to *E*g = 1.94eV for the as prepared product; the larger band gap of microflowers is most probably due to their the thinnest size effect of hierarchically interconnected nanosheets building blocks. Figure 6b shows the room temperature PL spectrum of hierarchical architectures of CuS. The emission spectrum was obtained with the excitation wavelength of 340nm. The as prepared CuS architectures exhibited a strong emission peak centered at 465nm, indicating the more nano size building blocks, much better highly crystalline and good optical feature of the as prepared CuS microflowers. Although Qin et al.[39] reported that there was no emission peak for CuS in the range of 400–800nm, our result is very consistent with the PL result reported by Ou et al.[40] and Kalyanikutty et al.[41] The size and morphology of the different CuS products may be responsible for the different phenomenon of emission, and the possibility of improvement in PL intensity due to higher crystallinity of microflowers cannot be ruled out. However, the origin of the observed optical properties is still far from well-understood, and more detailed investigations are needed.

To be a good candidate for a photo-catalyst, the larger surface area of the catalyst along cavities and hierarchical existence will result in higher photo-catalytic activity, so the specific surface area of photo-catalyst is crucial and most important factor. Since higher specific surface area can provide more active catalytic sites for photo-catalytic reactions. The Brunauer–Emmett–Teller (BET) specific surface area of synthesized CuS product was investigated by nitrogen adsorption-desorption measurements. Figure 6c shows the nitrogen adsorption-desorption isotherms of as prepared CuS microflowers. The BET surface area of the CuS hierarchical architectures was measured to be 61 m^2 g^{-1}. The surface area has been found to be much higher due to the special hierarchical existence of flowers along with the presence of cavities within the entire architecture of microflowers. Moreover the supreme and complex architectures of CuS microflowers appeared to be having double pore size having mesopores (Figure 6d). The unique double pore structures along with considerable high surface area makes a photo-catalyst promising candidate as a catalyst for the degradation of dye pollutions in wastewater.

Photo-catalytic properties

The optical system used for the photocatalytic reaction consisted of a 500 W Xenon lamp and a 420 nm cutoff filter (JB-420), which was placed under the reaction cell to completely remove all incoming wavelengths shorter than 420 nm to ensure irradiation with visible light only. Figure S5 illustrate the time- dependent absorption spectra of MB solution containing as prepared hierarchical microflowers in comparison with commercially available CuS powder as catalysts in the presence of hydrogen peroxide during the natural light irradiation.

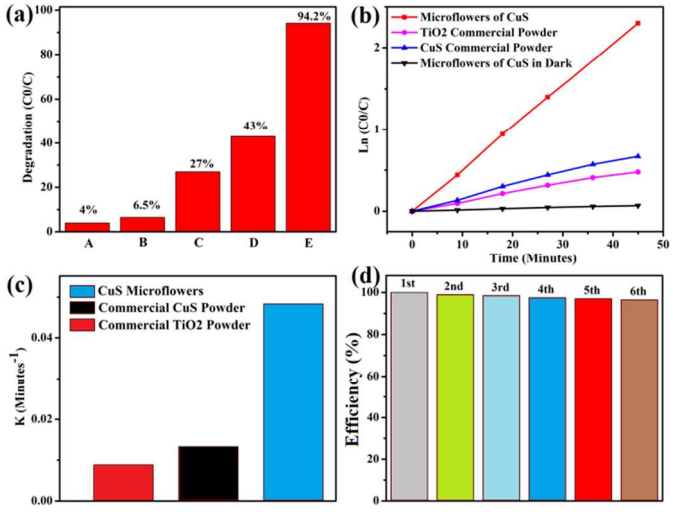

Figure 7 (a) A plot of the extent of photodegradation of MB by different catalysts under natural light. Panel A: Only H_2O_2 in the absence of any catalyst, Panel B: CuS microflowers + no H_2O_2, Panel C: commercial CuS powder + H_2O_2, Panel D: CuS microflowers + H_2O_2, (b The MB normalization concentration (from the optical absorbance measurements at 604nm) in the solution with different catalysts vs. the exposure time of the as prepared CuS microflowers and commercially available CuS powder and P25 under different conditions, (c) First order rate constant K (min^{-1}) of the as prepared CuS microflowers and commercially available CuS powder, (d) Stability test of as prepared CuS microflowers.

The characteristic absorption peak at 604nm of MB was used as a monitored parameter during the photo-catalytic degradation process. The catalytic property of CuS was found closely dependent to the amount of hydroxyl radicals; the assistance of H_2O_2 can be in favor of the bleaching of MB.[42] The H_2O_2 alone was found incapable to the degradation of dye solutions without the assistance of the catalyst (Figure S5a) and CuS catalyst without feeding H_2O_2 even after 45min of irradiation could degrade only 6.5% MB dye aqueous sloution (Figure S5b). Actually H_2O_2 yield highly reactive hydroxyl radicals that could oxidize RhB and MB into smaller molecules such as CO_2, H_2O, etc in the presence of CuS catalyst.[43] So the presence of H_2O_2 appeared to be necessary and crucial to assist the catalytic activity of the CuS.

Figure S5d shows the degradation of MB aqueous solution in the presence of H_2O_2 and as prepared CuS microflowers having hierarchically interconnected nanosheets as building blocks. The presence of CuS catalyst effectively accelerated the degradation of MB aqueous solution. The intensity of the absorption peak showed a rapid decrease with the extended exposure time. The degradation of MB dye solution was observed to be 38.7%, 57%, 74.5%, 85% and 94.2% after 9, 18, 27, 36 and 45min respectively (Figure S5d, Figure 7a; Panel D) and maintained at a relatively stable level after this time. Under similar degradation conditions the commercially available CuS and commercial TiO_2 (P25) powders (Figure S7) were also employed as catalyst in the presence of H_2O_2 and a precise comparison was carried out. The catalytic activity of CuS commercial powder and P25 was observed to be much slower, could degrade 43% and 27% MB solution within the same irradiation time (Figure S5c, Figure 7a; Panel C, Panel D). The decomposition of the MB aqueous solution within 45min of natural light irradiation in the presence of hierarchical microflower of CuS (94.5%) was found to be much higher than CuS commercial powder (43%) and P25 (27%) under the same typical degradation conditions. The relationship between Ln (C_o/C) and time for the as prepared CuS product and the CuS commercial powder and P25 is shown in Figure 7b. The catalytic activity of the CuS microflowers in the dark was also performed, which showed that only a little decrease in the concentration of MB was detected in the dark, which confirmed the concentration decrease of MB solution is mainly due to photodegradation of the products (Figure 7b). CuS hierarchical microflowers demonstrated photo-catalyst superiority over the as CuS commercially available powder and P25 as shown in Figure 7c, because the first order rate constant (K/min) of CuS microflowers (0.049247/min) is calculated to be much higher than the CuS commercial powder (0.013902/min) and P25 (0.00887/min) . First order rate constant is calculated by following equation.

$$Ln(C_o/C) = kt \quad (1)$$

Figure 7d display the as synthesized hierarchical microflowers to be having excellent stability and recycling capability. Almost same time was taken by CuS microflowers to degrade the MB dye aqueous solution without any significant loss of efficiency even for 6th cycle. In the recycling process, same catalyst was separated by centrifugation and used after washing for degradation of same concentration of MB dye aqueous solution under the same typical degradation conditions.

Figure S6 shows the degradation of RhB dye aqueous solution employing as prepared CuS microflowers with the assistance of H_2O_2 within 55min of natural light irridiation. The decomposition of the RhB dye aqueous solution in the presence of hierarchical microflowers of CuS (95%, Figure S6d, Figure 8c; Panel D) was also observed to be much greater than CuS commercial powder and P25 (Figure S6c, Figure S7b, Figure 8a; Panel C, Panel D). The relationship between Ln (C_o/C) and time for the as prepared CuS product and commercially available CuS powder and commercial P25 is shown in Figure 8b. The catalytic activity of the CuS microflowers in the dark was also performed, which showed that only a little decrease in the concentration of RhB was detected in the dark, which confirmed the concentration decrease of RhB solution is mainly due to photodegradation of the products (Figure 8b). The first order rate constant (K/min) of CuS microflowes (0.0487/min) was found to be much higher than CuS commercial powder (0.0136/min) and P25 (0.00762/min) (Figure 8c), demonstrating an excellent photocatalyst capability of as synthesised CuS microflowers. Moreover, the as synthesized microflowers appeared to be stable and recyclable catalyst in degrading the RhB dye aqueous solution as well (Figure 8d).

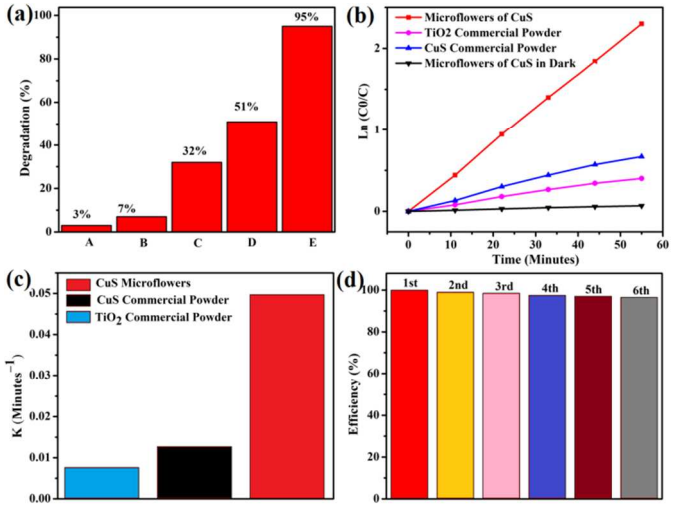

Figure 8 (a) A plot of the extent of photodegradation of RhB by different catalysts under natural light. Panel A: Only H_2O_2 in the absence of any catalyst, Panel B: CuS microflowers + no H_2O_2, Panel C: commercial CuS powder + H_2O_2, Panel D: CuS microflowers + H_2O_2, (b) The RhB normalization concentration (from the optical absorbance measurements at 604nm) in the solution with different catalysts vs. the exposure time of the as prepared CuS microflowers and commercially available CuS powder and P25 under different conditions, (c) First order rate constant K (min^{-1}) of the as prepared CuS microflowers and commercially available CuS powder and P25, (d) Stability test of as prepared CuS microflowers.

Figure 9 display the degradation of mixed solution of RhB and MB under similar conditions, as that for MB and RhB separately. Within the 50min of natural light irradiation the average removal of (MB+RhB) was found to be 93.5% and 41% for CuS microflowers, CuS commercial powder and commercial P25 respectively (Figure 9c, d, Figure S7c). H_2O_2 was also found to be crucial in degradation of mixed dyes solution (Figure 9a, b). Moreover, the as synthesized CuS microflowers were recycled 6 times for degradation of mixed dyes solution (MB+RhB) and results show its excellent stability and recycling capability, as shown in Figure 9f.

Overall the enhancement in the photo-catalytic property of as prepared CuS microflowers in the presence of H_2O_2 is most probably due to the fact; that, firstly H_2O_2 is a better electron acceptor than molecular oxygen, may increase the photo catalyzed rate by reducing the chances of electrons–holes recombination's.[44] Secondly, the active sites of the surfaces of CuS may catalyze the decomposition of H_2O_2 to generate a large number of hydroxyl radicals,[45] resulting in the enhancement of photodegradation efficiency. In a word, the improvement of degradation rate of aqueous dyes solutions relies on the synergistic effect of H_2O_2 and CuS.[46] The relevant chemical reactions include the separation of electron–hole pairs due to

irradiation and subsequent scavenging of these electrons and trapping of holes by H_2O_2 molecules.

$CuS + h\nu \rightarrow h_{vb+} + e_{cb}^-$ (5)

$H_2O_2 + h_{vb+} \rightarrow {}^{\cdot}OOH + H^+$ (6)

$H_2O_2 + e_{cb}^- \rightarrow {}^{\cdot}OH + OH^-$ (7)

${}^{\cdot}OOH \rightarrow {}^{\cdot}O_2^- + H^+$ (8)

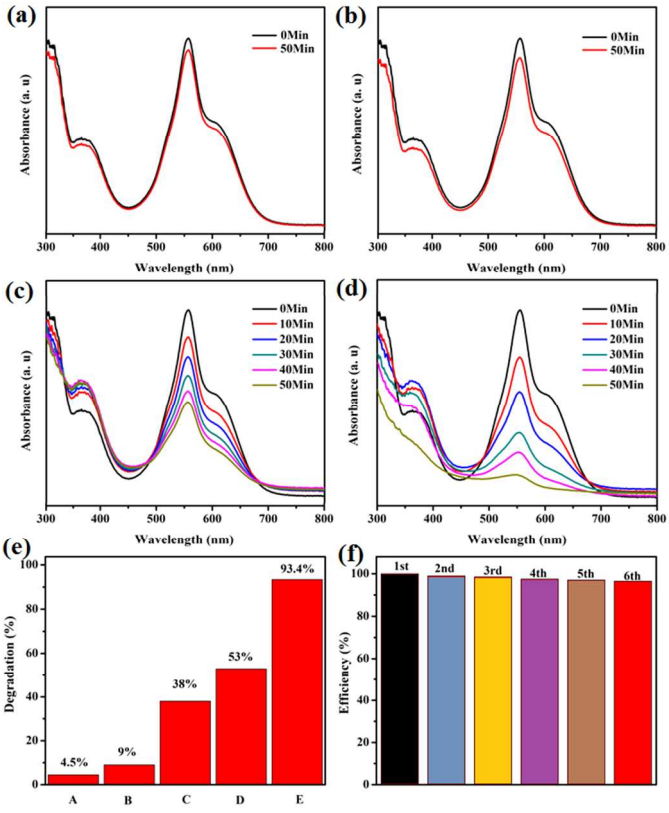

Figure 9. Absorption spectra of photo degradation of mixed dyes (MB+RhB) aqueous solution by different catalysts under natural light (a) without any catalyst + H_2O_2, (b) CuS microflowers + no H_2O_2, (c) commercial CuS powder + H_2O_2, (d) CuS microflowers + H_2O_2, (e) A plot of the extent of photodegradation of mixed dyes (MB+RhB) aqueous solution by different catalysts under natural light. Panel A: Only H_2O_2, Panel B: CuS microflowers + no H_2O_2, Panel C: commercial CuS powder + H_2O_2, Panel D: CuS microflowers + H_2O_2, (b) Stability test of as prepared CuS microflowers.

When the as prepared microflowers of CuS were irradiated with natural light in the presence of H_2O_2, holes present in the conduction band (CB) would be excited to the valence band (VB), with the simultaneous formation of electrons in the CB.[47] These electrons and holes can be captured by H_2O_2 molecules, so the formations of oxidants (equation (5)–(8)) taken place. That could oxidize RhB and MB into smaller molecules such as CO_2, H_2O, etc in the presence of CuS catalyst. The whole photodegradation mechanism is schematically illustrated in Figure 10. It has been demonstrated that because of their high oxidative capacities.[42] The photo generated oxidant species are in the favor of oxidizing organic contaminants.

Figure S8 shows the transient photocurrent responses of the samples under intermittent visible light illumination with the same wavelength range used in the photocatalytic reactions. It can be seen that the the photocurrent significantly and rapidly decreases as long as the light is switched off. It is known that the photocurrent is produced mainly by the diffusion of the photogenerated electrons to the ITO, and meanwhile the photoinduced holes are taken up by the hole acceptors in the electrolyte.[48] Therefore, the enhanced photocurrent indicates a more efficient separation of the photoexcited electron–hole pairs or a longer lifetime of the photogenerated charge carriers. This photogenerated charge separation efficiency has also been confirmed before by the photoluminescence (PL) spectra.

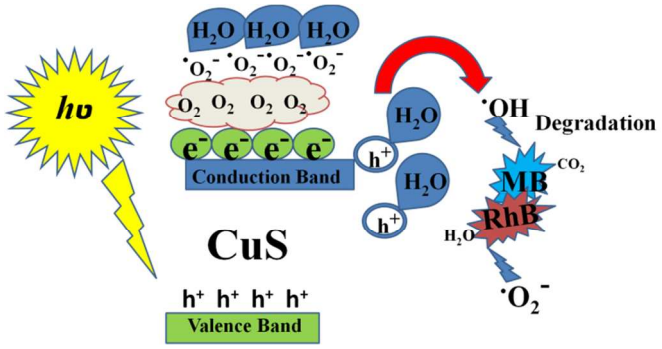

Figure 10. Schematic illustration of the photodegradation of MB and RhB.

In addition, other electrochemical analysis, including electrochemical impedance spectroscopy (EIS) has also been carried out. As shown in Figure S9, the Nyquist plots of the CuS electrode materials cycled in 0.2 M Na_2SO_4 electrolyte solution show semicircle at high frequencies. Since the preparation of the electrodes and electrolyte used is alike, the high-frequency semicircle is related to the resistance of the electrodes. In the Nyquist plot, the high-frequency corresponds to the charge transfer limiting process and can be attributed to the double layer capacitance (C_{dl}) in parallel with the charge transfer resistance (R_{ct}) at the contact interface between the electrode and the electrolyte solution. The Equivalent Series Resistance (ESR) can be determined from the intercept of curve in the high frequency region on x-axis. ESR includes resistance of active material, solution resistance and contact resistance of active material with electrode. The calculated ESR is 0.57 ohm represents very low resistance of our three electrode configuration (inset of Figure S9).[49]

It is concluded that the photo-catalyst activity of the CuS microflowers in degrading highly concentrated dyes (MB, RhB, MB+RhB) aqueous solution is much higher than that of the commercially available CuS powder. The highest photo-catalytic activity of CuS microflowers is due to at least the following several factors. Firstly, the microflowers have the largest surface area (61 $m^2 g^{-1}$) due to their entire hierarchical existence with the thinnest nanosheets building blocks and unique double pore sizes. Since the CuS microflowers are in the supreme hierarchical existence and extremely enriched by nanosheets building blocks. So, it is generally acceptable that the microflowers can provide more active catalytic sites for photo-catalytic reactions.[50] Secondly, the hierarchical microflowers due to a lot of unfolded and extremely thinnest nanosheets possess plenty of pores within the hierarchically interconnected nanosheets, which not only reduce reflection and harvest more light, can also contribute to the transport for the molecules of organic contaminants to get to the active sites on inner sides as well.[51] So the nanosheets could absorb more photons to produce electron–hole pairs under natural light,[50] and these deep and capacious pores enable the hierarchical structures to be exposed to the dye solutions sufficiently. Furthermore, the nano-size of sheets could reduce the radiationless recombination of electron–hole

pairs,[51] which is also in favor of the enhanced photocatalysis of highly concentrated dyes solutions.
Thus, it is excellently believable that the photo-catalytic superiority of the as prepared CuS microflowers with hierarchically interconnected nanosheets as building blocks is attributed to their high specific surface area, wholly exposed and hierarchical existence, excellent dispersing and uniformity. Moreover, the versatile photo degradation of organic dyes carried out under the natural light suggests the potential application to be quite feasible in practice.

Conclusions

In summary, the sonochemical synthesis of CuS hierarchical architectures fully exposed with thinnest nanosheets as building blocks has been successfully achieved. The extra ordinary versatile photo-catalytic capability of the as-prepared hierarchical CuS microflowers with rather high surface area have been attributed to their active components of nanosheets building blocks and entirely isolated existence. The present study not only opens a new horizon for the synthesis of entirely isolated and complex morphologies based on nanosheets building blocks with fully exposed surfaces for many other chalcogenides, also is of fundamental importance for the investigation of their potential applications in other fields, including sensors, optics, and so forth.

Acknowledgements

This work was supported by National Natural Science Foundation of China (21371023, 50972017) and the Research Fund for the Doctoral Program of Higher Education of China (20101101110026).

Notes and references

[1]Research Centre of Materials Science, Beijing Institute of Technology, Beijing 100081, P. R. China
[2]Institute of Physics & Institute of Micro- and Nanotechnologies (ZIK MacroNano), Technische Universität Ilmenau, 98693 Ilmenau, Germany.
[3]Department of Materials Science and Engineering, College of Engineering, Peking University Beijing 100871, China.

1. Xiaoyang Pan, MinQuan Yang, Xianzhi Fu, Nan Zhang and YiJun Xu, *Nanoscale*, 2013, **5**, 3601. (b) Manoj A. Lazar and Walid A. Daoud, *RSC Adv*., 2013, **3**, 4130. (c) Wee-Jun Ong, Lling-Lling Tan, Siang-Piao Chai, Siek-Ting Yong and Abdul Rahman Mohamed, *Nano Research*, 2014, **7**, 1528. (d) Liu Lichen, Liu Zhe, Liu Annai, Gu Xianrui, Ge Chengyan, Gao Fei, Dong Lin, *ChemSusChem*, 2014, **7**, 618.
2. Yu Xuelian, Chuanbao Cao, Hesun Zhu, *Advanced Functional Materials*, 2007, **17**, 1997. (b) J. Liu and D. F. Xue, *J. Mater. Chem.*, 2011, **21**, 223-228.
3. (a) X.L. Yu, Y. Wang, H.L.W. Chan, C. B. Cao, *Microporous and Mesoporous Materials*, 2009, **118**, 423.(b) Nasir Mahmood, Muhammad Tahir Asif Mahmood, Jinghan Zhu, Chuanbao Cao Yanglong Hou, *Nano Energy*, 2015,**11**,267.
4. Muhammad Tahir, Chuanbao Cao, Faheem K. Butt, Faryal Idrees, Nasir Mahmood, Zulfiqar Ali, Imran Aslam, M. Tanveer, *J. Mater. Chem. A*, 2013, **1**, 13949. (b) Faryal Idrees, Chuanbao Cao, Faheem K. Butt, Muhammad Tahir, M. Tanveer, Imran Aslam, Zulfiqar Ali, Tariq Mahmood and J. Hou, *CrystEngComm*, 2013, **15**, 8146. (c) F. Idrees, C. Cao, F. K. Butt , M. Tahir, I. Shakir, M. Rizwan, I. Aslam, M. Tanveer, Z. Ali, *Int. Journal of hyd. Energy*, 2014, **39**, 13174
5. J. S. Zhou, H. H. Song, X. H. Chen, L. J. Zhi, S. B. Yang, J. P. Huo and W. T. Yang, *Chem. Mater.*, 2009, **21**, 2935-2940.
6. J. Liu, S. Z. Qiao, S. B. Hartono and G. Q. Lu, *Angew. Chem. Int. Edit.*, 2010, **49**, 4981-4985.
7. Muhammad Tahir, Chuanbao Cao, Nasir Mahmood, Faheem K. Butt, Asif Mahmood, Faryal Idrees, Sajad Hussain, M. Tanveer, Zulfiqar Ali, Imran Aslam, *ACS Appl. Mater. Interfaces*, 2014, **6**, 1258. (b) I. Aslam, C. Cao, M. Tanveer, W. S. Khan, M. Tahir, M. Abid, F. Idrees, F. K. Butt, Z. Ali and N. Mahmood, *New J. Chem*., 2014, **38**, 5462. (c) I. Aslam, C. Cao, W. S. Khan, M. Tanveer, M. Abid, F. Idrees, R. Riasat, M. Tahir, F. K. Butt and Z. Ali, *RSC Adv*., 2014, 4, 37914. (d) M. Tanveer, C. Cao, I. Aslam, Z. Ali, F. Idrees, W. S. Khan, F. K. Butt, M. Tahir and A. Mahmood, *Sci.of Adv. Mater.*, 2014, **6**, 1.
8. (a) Zulfiqar Ali, Chuanbao Cao, Jili Li, Yanli Wang, Tai Cao, M. Tanveer, Muhammad Tahir, Faryal Idrees, Faheem K. Butt, *Journal of Power Sources* 2013, **229**, 216. (b) Zulfiqar Ali, Misbah Mirza, Chuanbao Cao, Faheem K. Butt, M. Tanveer, Muhammad Tahir,Imran Aslam, Faryal Idrees, Muhammad Safdar, *ACS Appl. Mater. Interfaces*, **2014**,*6*,9550.
9. M. Luo, Y. Liu, J. C. Hu, J. L. Li, J. Liu and R. M. Richards, *Appl. Catal. B Environ.*, 2012, **125**, 180-188. (c) Muhammad Tahir, Chuanbao Cao, Faheem K. Butt, Sajid Butt, Faryal Idrees, Zulfiqar Ali, Imran Aslam, M. Tanveer, Asif Mahmood and Nasir Mahmood, *CrystEngComm*, 2014, 16,1825.
10. Q. Liu, H. Liu, M. Han, J. Zhu, Y. Liang, Z. Xu and Y. Song, *Adv. Mater.*, 2005, **17**, 1995.
11. D. Walsh, B. Lebeau and S. Mann, *Adv. Mater.*, 1999, **11**, 324.
12. S. D. Sun, X. P. Song, C. C. Kong, S. H. Liang, B. J. Ding and Z. M. Yang, *CrystEngComm*, 2011, **13**, 6200-6205.
13. S. S. Dhasade, S. Patil, B. B. Kale, S. H. Han, M. C. Rath and V. J. Fulari, *Mater. Lett.*, 2013, **93**, 316-318.
14. X. Y. Meng, G. H. Tian, Y. J. Chen, R. T. Zhai, J. Zhou, Y. H. Shi, X. R. Cao, W. Zhou and H. G. Fu, *CrystEngComm*, 2013, **15**, 5144- 5149.
15. M. Tanveer, Chuanbao Cao, Waheed S. Khan, Zulfiqar Ali, Imran Aslam, Faheem K. Butt, Faryal Idrees, Muhammad Tahir and Nasir Mahmood, *CrystEngComm*, 2014, **16**, 5290-5300. (b) M. Tanveer, Chuanbao Cao, Imran Aslam, Zulfiqar Ali, Faryal Idrees, Muhammad Tahir and Asif Mahmood, *RSC Adv.*, 2014, **4**, 63447. (c) Faryal Idrees, Chuanbao Cao, R. Ahmed, Faheem K. Butt, Sajid butt, Muhammad Tahir and M. Tanveer, *Sci.of Adv. Mater*.doi: 10.1166/sam.2014.2044.
16. L. Zhao, F. Q. Tao, Z. Quan, X. L. Zhou, Y. H. Yuan and J. C. Hu, *Mater. Lett.*, 2012, **68**, 28- 31.
17. J. Liu and D. F. Xue, *J. Cryst. Growth*, 2009, **311**, 500-503.
18. J. G. Yu, J. Zhang and S. Liu, *J. Phys. Chem*., 2010, **114**, 13642.
19. Yu, J. G., Hai, Y., Cheng, B. *J. Phys. Chem. C*, 2011, **115**, 4953.
20. Ghijsen, J., Tjeng, L. H., Elp, J. V., Eskes, H.; Westerink, J., Sawatzky, G. A.; Czyzyk, M. T. *Phys. Rev. B*, 1988, **38**, 11322.
21. Todd, E. C., Sherman, D. M. *Am. Mineral*., 2003, **88**, 1652.
22. F. Li, J. F. Wu, Q. H. Qin, Z. Li and X. T. Huang, *Powder Technol*., 2010, **198**, 267**.**
23. Jixiang Fang, Bingjun Ding, and Xiaoping Song, *crystal growth & design* 2008, **8**, 3616.
24. X. Y. Chen, Z. H. Wang, X. Wang, R. Zhang, X. Y. Liu, W. J. Lin and Y. T. Qian, *J. Cryst. Growth*, 2004, **263**, 570-574.
25. J. Z. Xu, S. Xu, J. Geng, G. X. Li and J. J. Zhu, *Ultrason. Sonochem.*, 2006, **13**, 451-454.
26. C. H. Deng and X. B. Tian, *Mater. Res. Bull.*, 2013, **48**, 4344-4350.
27. R. Vijaya Kumar, Y. Diamant and A. Gedanken, *Chem. Mater.*, 2000, **12**, 2301-2305.
28. M. Kristl, N. Hojnik, S. Gyergyek and M. Drofenik, *Mater. Res. Bull.*, 2013, **48**, 1184-1188.
29. Z. Li, L. W. Mi, W. H. Chen, H. W. Hou, C. T. Liu, H. L. Wang, Z. Zheng and C. Y. Shen, *CrystEngComm*, 2012, **14**, 3965-3971.
30. W. W. He, H. M. Jia, X. X. Li, Y. Lei, J. Li, H. X. Zhao, L. W. Mi, L. Z. Zhang and Z. Zheng, *Nanoscale*, 2012, **4**, 3501-3506.

31. M. Basu, A. K. Sinha, M. Pradhan, S. Sarkar, Y. Negishi, G. and T. Pal, *Environ. Sci. Technol.*, 2010, **44**, 6313-6318.
32. Y.Y. Hu, A. Rawal, K. Schmidt-Rohr, Proc. *Natl. Acad. Sci*. 2010, **107**, 22425.
33. Baoquan Xie, George H. Nancollas, Proc. *Natl. Acad. Sci*. 2010, **107**, 22369.
34. M.T.S. Nair, P.K. Nair, Semicond. Sci. Technol.1989, **4**, 191.
35. Zhang, P. Gao, L. *J. Mater.Chem*., 2003, **13**, 2007.
36. Gao, J. Li, Q. Zhao, H. Li, L. Liu, C. Gong, Q. Qi, L. *Chem. Mater*., 2008, **20**, 6263.
37. Chen, L. Yu, W. Li, Y. *Powder Technology*, 2009, **52**, 191.
38. S. K. Haram, A. R. Mahadeshwar, S. G. Dixit, *J. Phys. Chem*., 1996, **100**, 5868.
39. A. M. Qin, Y. P. Fang, H. D. Ou, H. Q. Liu, C. Y. Su, *Cryst. Growth Des*., 2005**, 5**, 855.
40. S. M. Ou, Q. Xie, D. K. Ma, J. B. Liang, X. K. Hu, W. C. Yu, Y. T. Qian, *Mater. Chem. Phys*., 2005, **94**, 460.
41. K. P. Kalyanikutty,M. Nikhila, U. Maitra, C. N. R. Rao, *Chem. Phys. Lett*., 2006, **190**, 432.
42. J. Shi, J. Li, X. J. Huang and Y. W. Tan, *Nano Res.*, 2011, **4**, 488.
43. H. Xu, W. Wang and W. Zhu, *J. Phys. Chem. B*, 2006, **110**, 13829.
44. D. F. Ollis, E. Pelizzetti, N. Serpone, *Environ. Sci. Technol*., 1991, **25**, 1522.
45. J. L. Elechiguerra, J. R. Gasga and M. J. Yacaman, *J. Mater. Chem*., 2006, **16**, 3906.
46. T. Y. Wei, Y. Y. Wang, C. C. Wan, *J. Photochem. Photobiol*. A,, 1990, **55** 115.
47. Z. H. Wang, S. P. Zhao, S. Y. Zhu, Y. L. Sun and M. Fang, *CrystEngComm*. 2011, **13**, 2262.
48. S. Soedergren, A. Hagfeldt, J. Olsson and S.E. Lindquist, *J. Phys. Chem*., 1994, **98**, 5552.
49. J. W. Ondersma and T. W. Hamann, *Langmuir*, 2011, **27**, 13361.
50. L. Zhang, H. Yang, J. Yu, F. Shao, L. Li, F. Zhang, H. Zhao, *J. Phys. Chem. C*, 2009, **113**, 5434.
51. G. Tian, Y. Chen, W. Zhou, K. Pan, Y. Dong, C. Tian and H. Fu, *J. Mater. Chem*., 2011, **21**, 887–892.